Where Are the "Earth-like Planets"? On the Predictive Power of Geometrodynamic Models

Anatoly V. Belyakov

Tver, Russia. E-mail: belyakov.lih@gmail.com

Physical models based on J. Wheeler's geometrodynamics, when applied to planetary systems and pulsars, agree well with modern observational results and predict new ones. The current geometrodynamic model explains the appearance of the "hot Neptunian desert" region, the existence of an "airy super-Earth", the construction of compiled pulsar spectra, the calculation of their "death line", the calculation of braking indices for various pulsar populations, and much more.

1 Introduction

As is known, geometrodynamic models are capable of predicting and yielding results that, in some cases, are currently unattainable by theories based on the mathematical apparatus of theoretical physics, especially if these theories are based on an inaccurate physical model of the object.

Besides, geometrodynamic models examine the organisation of material space (medium) into objects, *regardless of their specific substance and behavior*, which is already the subject of study in specialized disciplines. Only the presence of this organisation (order) of the environment, which creates certain types of structures and determines their evolution, is significant. In particular, schematic models of objects are considered, the evolution of which depends only on a very few parameters that manifest the most important properties of real bodies, in this case — cosmic bodies.

Recall that these models are constructed using balances between the fundamental interactions: electrical, magnetic, gravitational, and inertial ones. This ensures their logical correspondence with natural physical laws. This is supported by examples in addition to works [1,2] concerning planetary systems and pulsars.

2 Planetary systems

Earth-like planets, given their masses and distances from their central star, have not yet been discovered, with the possible exception of Kepler 452b. However, they should not exist, as despite the enormous diversity and statistical spread of planetary parameters and planetary system parameters, certain patterns do exist, as outlined in the author's 2014 paper [1].

The results and conclusions of [1] are increasingly reinforced by the discovery of new exoplanets. Specifically, there are two types of planetary systems: the former formed from flat-spiral protoplanetary clumps of matter, while the latter are formed from lenticular ones. This conclusion should have been reached long ago, if only because protostellar clumps of matter also organize into spiral and elliptical (lenticular) galaxies. The analogy is entirely appropriate, as gravitational and magnetic forces are at work in both cases.

In planetary systems of the first type, the mass of the planets increases with distance from the star, while in planetary systems of the second type, it decreases (see Fig. 1). For planets of the first type, the dependence of the planet's mass m on the radius of its orbit r and the mass of the central body M has been derived:

$$m = \left(rM^2\right)^{4n/(5n-1)}, \tag{1}$$

and for planets of the second type, respectively:

$$m = \left(\frac{M}{r}\right)^{4k}, \tag{2}$$

where n is a coefficient close to 1, and k is a coefficient close to $\frac{1}{3}$. That is, hot Jupiters form naturally near their star, rather than migrating from distant orbits.

Thus, the mass-radius region is unevenly populated by planets, and features appear on the $m(r)$ diagram, namely, clumps of cold and hot Jupiters (the intersections correspond to their coordinates for a solar-mass star), a "desert of hot Neptunes", and others. Moreover, in the second case, if planets do appear on the periphery of the lenticular disk, they have very low densities.

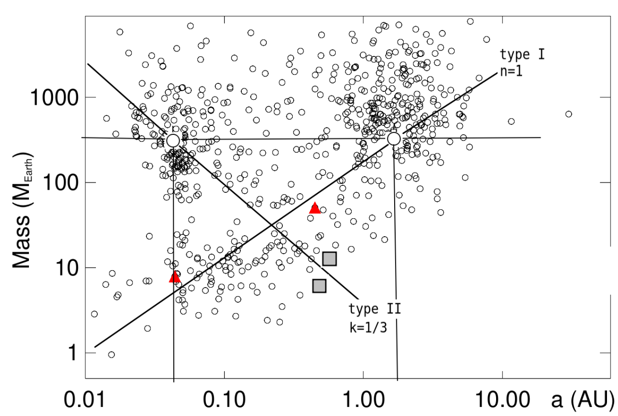

Fig. 1: The calculated dependence $m(r)$ on the background of distribution of all known extrasolar planets in the semimajor axis-mass parameter spaces. Triangles represent the planets of the system GJ 221. The squares show the planets of the TOI-791 system. The masses shown in masses of the Earth.

As follows from the figure, for a solar-mass star, it would be more likely to have a giant planet appear at a distance of about 1 AU in the first case, or an "airy" super-Earth in the second. Indeed, according to the latest data, planets TOI-791 b and TOI-791 c, which have very low densities, are located on the evolutionary line of type II planets [3]. Their locations and relationships according to (1) and (2) are shown in the diagram borrowed from [4] (for higher stellar masses, the $m(r)$ relationships shift upward, and vice versa).

These findings were actually predicted by the author in already 2014, given that the paper [1] was published in 2014.

Therefore, our planetary system represents a rare case in which Earth-like planets, formed in close proximity to the Sun, migrated into existing orbits. Therefore, Earth-like planets should be sought in systems with massive planets in distant orbits.

3 Pulsars

Cosmological objects, and pulsars in particular, have a very wide range of parameters due to their different ages and other factors. Therefore, to cover their evolutionary range, two parameters, k and j, were introduced. $k = \frac{2}{3} \ldots 1$ is a parameter that characterizes the state of the medium comprising the object and its change on the evolutionary diagram, and $j = \frac{1}{3} \ldots 1$ determines the shape reflecting the object's dimensionality (for more details, see [2]). No additional coefficients were introduced.

In [2], the author had theoretically obtained various pulsar parameters. Some of these, it should be emphasized, are currently absent or exist only as correlations or model spectra requiring a number of empirical coefficients.

In the author's model, all dependencies are expressed only through the dimensionless mass of the pulsar M_p and the aforementioned parameters k and j, while all other coefficients are ratios of fundamental or known quantities, the derivation of which can be traced in the work [2]. Below are examples of the use of these formulae in relation to pulsars.

3.1 Radio pulsar luminosity limits

The simplest radio pulsar is a vortex tube, by definition "immersed" in the Y region. The vortex tube is a macrooscillator or emitter, with coherent radiation generated and amplified along the entire length of the vortex tube by an antenna mechanism.

The formulae for calculating the radiation power and period of a pulsar are as follows:

$$N_p = 1.45 \times 10^{20}\, M_p^{4/3-2k} \text{ Watts}, \tag{3}$$

$$P = 282.5\, M_p^{2k/3} \text{ sec}, \tag{4}$$

where the mass M_p is taken as generally accepted, i.e., 1.4 solar masses or $2.8{\times}10^{-6}$ of the characteristic mass M_m, equal to $\frac{1}{\gamma} R_c c^2$, where R_c is the characteristic size derived from the balance of electric and magnetic forces, equal to $7.52{\times}10^{8}$ m.

The dimension coefficient for N_p is

$$\frac{\sigma (T_k \lambda_k R_c)^4}{f^2 r_e^6}\,,$$

where σ is the Stefan-Boltzmann constant, λ_k and T_k are the Compton wavelength and the temperature corresponding to it, f is the ratio of electric forces to gravitational forces, r_e is the classical radius of the electron (the other coefficients in front of M_p are expressed similarly).

Thus, this model *predicts* the existence of a lower limit on the radiation power of radio pulsars at $k \to \frac{2}{3}$, which the pulsar approaches as the medium degrades and its rotation rate slows down. In this case, $N_{\min} = 1.45 \times 10^{20}$ W and does not depend on the pulsar mass, and for $k = 1$, expression (3) gives an upper limit on N_p, which depends on the pulsar mass, and these limits actually exist [5, 7]. At luminosities below $N_{\min}$, pulsars are not detected, and while the upper limit on the luminosity can be explained by the complete conversion of the pulsar rotation energy into radiation, the lower limit is not numerically determined by existing theories.

3.2 Compilation spectra

Pulsar radio emission covers a wide range and is extremely heterogeneous in time, intensity, and frequency. However, there are stable average spectra of the energy distribution over frequency, obtained by numerous instant measurements of the emission over long periods of time at various frequencies. These averaged spectra differ in their position and shape in the energy-frequency coordinate system.

A real pulsar differs from the simplest model of a single vortex tube because, like its real physical counterpart in a fluid (a vortex structure), it not only rotates but also changes its configuration along the Y-axis: from a vortex tube ($j = 1$, a conventionally one-dimensional state) to a vortex funnel on the surface ($j = \frac{1}{3}$, a conventionally three-dimensional state or quasi-sphere), which is reflected in the shape and position of the spectra.

In [2], the parameters for this general case are defined: the radiation energy, the radiation power, and the pulsar period:

$$E_p = 511\, M_p^{1.454k-0.7575} \text{ keV}, \tag{5}$$

$$N_p = 1.22 \times 10^{38}\, M_p^{6.15k-2.7} \text{ Watts}, \tag{6}$$

$$P = 2.51\, M_p^{0.7575-1.454k+j} \text{ sec}. \tag{7}$$

Note that for $k = 0.75$ and $j = \frac{1}{3}$, the exponent of M_p in (7) is zero and $P = (2\pi)^{1/2} = 2.51$ sec, a period that is the same for any mass.

The relationship between the maximum radiation frequency and the period in this model is:

$$\nu = \frac{c^{1/2}}{2\pi \lambda_k^{1/2} P^{1/2}} \text{ Hz}, \tag{8}$$

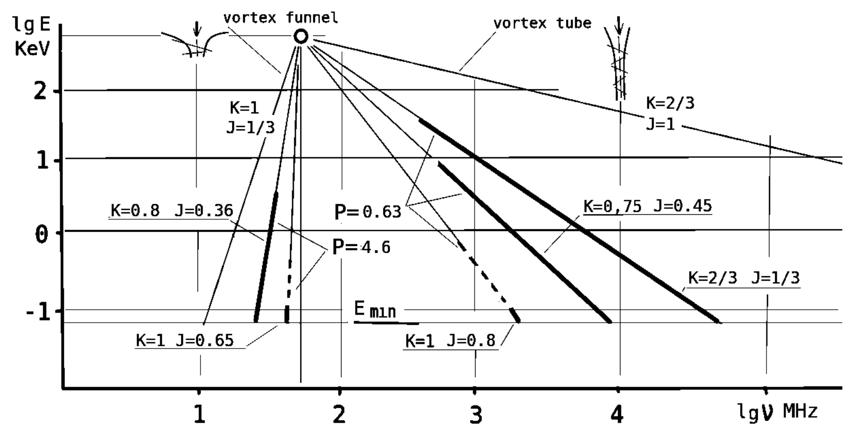

Fig. 2: Scheme of formation of average spectra of pulsars.

and from equations (5) and (7), keeping in mind (8), the dependence $E_p(\nu)$ is derived:

$$\nu = (2\pi)^{-1.25} c^{1/2} \lambda_k^{-1/2} \left(\frac{E_p}{511}\right)^{-\frac{1}{2}\frac{0.7575-1.454k+j}{1.454k-0.7575}}. \qquad (9)$$

It has been established that the average spectrum has an energy maximum shifted toward lower frequencies [5]. This fact can be explained, based on our model, by the existence of an optimal packing dimension of vortex filaments in the pulsar's vortex tube, less than 3, at which the pulsar remains relatively longer. In [6], it is indicated that this optimal dimension could be a fractal dimension of $e = 2.72$, so that ultimately, changing the packing dimensions leads to a shift of the spectrum toward lower frequencies by approximately 1.3 logarithmic units, Fig. 2.

The region of existence of average spectra is limited by logarithmic straight lines according to (9) with exponents $k = 1$, $j = \frac{1}{3}$ and $k = \frac{2}{3}$, $j = 1$, emanating from the point with coordinates: $E_p = 511$ MeV, $\nu = 51.4$ MHz. Real spectra are located in this region, and they, as a rule, have, according to the accepted terminology, a low-frequency cutoff, a maximum and a linear section, breaking off at a high-frequency break.

A pulsar exists in various configurations and, while having a constant period, radiates at different frequencies and energies due to different combinations of the parameters k and j. As an example, Fig. 2 shows the calculated positions of some beams that form the spectra of two pulsars with periods: left $P = 4.6$ sec (two rays), right 0.63 sec (three rays). The values of the parameters k and j are indicated in the Figure. For the left pulsar, its radiation gravitates toward the low-frequency cutoff region and ends abruptly in the high-frequency bend region; for the right pulsar, its radiation gravitates toward the high-frequency break region and ends abruptly in the low-frequency cutoff region. The beams are limited by maximum and minimum energies as the parameter k varies in accordance with formula (5). It should be noted that, as noted in [5], characteristic spectral features (kinks, dips) may be absent or fictitious in many cases.

Thus, the pulsar's existence in various configurations during its pulsations along the Y-axis, with constant changes in the state of its material medium (parameter k) and shape (parameter j), ultimately leads to the emergence of its individual average spectrum, which is closest to the configuration in which the pulsar spends the longest time. Of course, equation (9) cannot reproduce the spectral shape of specific pulsars, but it fully explains their features, and the shape of the calculated spectrum is entirely consistent with the modeled spectra provided in [5].

3.3 On the parameters of pulsars

In addition to the above, an important parameter of a pulsar is its magnetic force B. In [2], formulae for a conventional radio pulsar are derived

$$B = 1.27 \times 10^{-4}\, M_p^{k/3 - 2j - 2/3} \text{ Gauss}, \qquad (10)$$

and for a pulsar with a large magnetic force (excited state):

$$B_m = 2.1 \times 10^{5}\, M_p^{-j - 2/3} \text{ Gauss}. \qquad (11)$$

Pulsars have a very wide spread of their parameters, so their two-parameter dependencies are not calculated; only approximate correlations exist. The calculated solution regions for some parameters are presented in [2].

Additionally, as an example, Fig. 3, borrowed from a recent paper [7], superimposes the solution regions in the ($\lg B$, $\lg P$) coordinates, bounded by the limiting values of the parameters k and j for pulsars with a high magnetic force (upper region) and ordinary pulsars (lower region), calculated using equations (7), (10), and (11). In turn, these regions are bounded by the "death line", which, according to the latest data (dashed line), corresponds to a luminosity of 10^{28} erg/s (10^{21} W), which is precisely *what our model predicts*; however, existing theories disagree on the causes of pulsar attenuation and do not provide a definitive value for their minimum luminosity.

The region of millisecond pulsars with a large magnetic

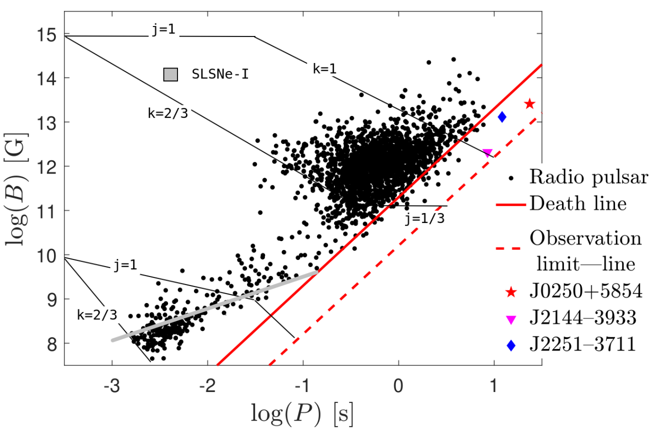

Fig. 3: The magnetic field versus period (B–P) diagram for the radio pulsars. The solid line is the death line defined as $B_{12}/P^2 \simeq 0.2$ (e.g., Ruderman & Sutherland 1975; Bhattacharya & van den Heuvel 1991), and the dashed line is the "observational limit — line" corresponds to $\dot{E} \simeq 10^{28}$ erg/sec. The pulsar samples are taken from the ATNF Pulsar Catalogue.

force is not filled, however, such pulsars (magnetars) exist, and *this fact can be considered predicted by this model*, since a magnetar was recently discovered in a supernova (this is SLSNe-I, the magnetar spin period to $P = 4.2 \pm 0.2$ ms and the magnetic-field strength to $B = (1.6 \pm 0.1) \times 10^{14}$ Gauss [8]), its position is indicated by a square.

Note that for pulsars with a low magnetic force, when their structure is close to the single vortex tube model ($j = 1$), the mutual solution of equations (3) and (4) with the exclusion of the parameter k, together with (10), yields the dependence

$$B = 1.27 \times 10^{-4}\, M^{\frac{\lg P - 2.45}{2 \lg M} - 2j - 2/3}, \qquad (12)$$

which correlates with the array of short-period pulsars (grey line).

A key characteristic of pulsars is the dependence of the period derivative on the period, $dP/dt(P)$, since this parameter is used to calculate the magnetic force and energy loss during pulsar deceleration. Furthermore, individual pulsar groups (clusters) have their own distinctive features and differ in the average derivative value, its sign, slope, rotational deceleration rate, etc., some of which remain unexplained [5, 9, 10].

For example, I. F. Malov points out that the entire known array of pulsars cannot be described by a single magnetodipole model. In particular, the $dP/dt(P)$ dependence in normal long-period pulsars is inconsistent with the magnetodipole braking model and requires the use of other mechanisms or a search for specific distributions of their parameters. However, this model is valid for pulsars with $P > 2$ sec, which have strong magnetic fields.

These differences are not entirely clear within existing theories, but are fully explained in terms of the geometrodynamic model. Thus, the general classification of pulsars

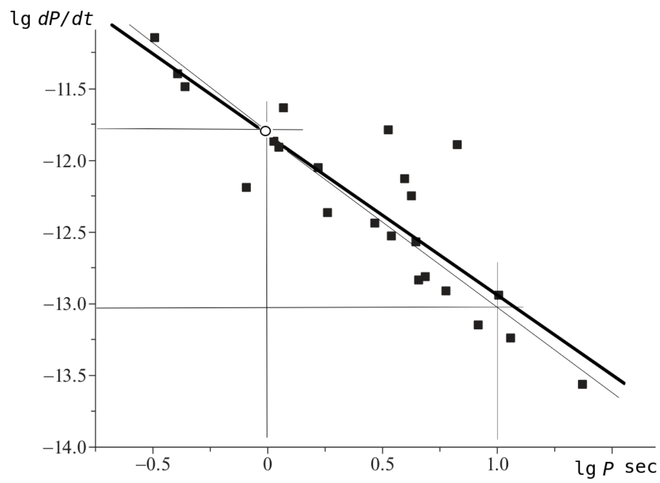

Fig. 4: Dependence of the period derivative on the period for pulsars with $B_s > 2.2 \times 10^{13}$ Gauss (based on [9]).

into periods greater or less than two seconds is related to the change in sign of the exponent in equation (7) at $P \sim 2$ sec. If $P < 2$ sec, then the exponent in formula (7) is positive; for $P > 2$ sec, it is negative. This feature is also reflected in the shape of the average spectra, see Fig. 2.

Moreover, the pulsar gradually loses its mass, and, as follows from formula (7), a negative exponent leads to an increase in the period, i.e., *promotes pulsar braking*, while a positive exponent *decreases the period and hinders braking*.

For normal pulsars (vortex tubes), according to (4), the exponent is always positive. However, for pulsars with $P > 2$ sec, which have large magnetic fields and whose period is calculated according to (7), the exponent is negative. This difference is reflected in the sign of the derivative $dP/dt(P)$ for different pulsar types.

The derivative dP/dt is determined from observations of the arrival times of pulses from the pulsar; in our case, since pulsars continuously change their position on the evolutionary diagram (for more details, see [2]), its analog is the derivative of the period with respect to the parameter k, dP/dk. Differentiating formulae (4) and (7), we obtain — for a normal radio pulsar

$$dP/dk = 188\, \ln M_p \times M_p^{2k/3}, \qquad (13)$$

and for a pulsar in the general case and, in particular, with a large value of B

$$dP/dk = -3.65 \ln M_p \times M_p^{0.7575 - 1.454k + j}. \qquad (14)$$

Assuming that these derivatives are proportional to the time derivatives, we can determine the slope of the $dP/dt(P)$ dependence. Thus, the ratios of the dP/dk derivative to the period P (i.e., their second derivatives with respect to k) for normal pulsars are (−8.5), for the general case it is 18.6; their common logarithms 0.93 and (−1.27) are the *braking indices of pulsar* (n). Thus, to obtain these indices, an observational data set $dP/dt(P)$ is not required, and *a single point is sufficient* to construct the correlation.

In confirmation, Fig. 4 shows the $dP/dt(P)$ dependence according to [9] for pulsars with a large magnetic field, where the calculated index -1.27 (thin line) is in good agreement with the correlation of the data array (bold line); and the index 0.93 corresponds to the dependence for normal pulsars (see also [9]). Moreover, in [11] for arrays of second and millisecond pulsars, the average value $n = 0.92 \ldots 0.94$ was established, **which exactly coincides with the calculated one**!

Of course, these cases do not exhaust the behavior of pulsars. For example, if the medium forming the pulsar or cluster does not evolve, then changes in the pulsar can only affect its dimension (shape); then, similarly, differentiating with respect to the parameter i with k constant, equation (7) and so on, we ultimately obtain $n = 1.1$.

Finally, if both parameters k and j are constant and only M_p changes, then differentiating P with respect to M and following similar transformations, we obtain the formula for the braking index:

$$n = \lg\left[(0.7575 - 1.454k + j)\, M_p^{-1}\right]. \tag{15}$$

In this case, the index, depending on the combination of parameters k and j, can take values (rounded) from -5 to 5; so that the **calculated boundary value coincides with the theoretical value of the index** ($n = 5$) for a pulsar slowing down its rotation solely due to the emission of gravitational waves from the quadrupole mode of the main mass [12].

Apparently, this is precisely the case for a large group of pulsars "crowded" on the $dP/dt(P)$ diagram in the interval of $0.3 \ldots 3$ seconds [9], i.e., a period close to the change in sign of the exponent at P in formula (7). Indeed, with small variations in the properties of the medium and the shape of the pulsar, its evolution will mainly depend on the loss of its mass with a constant change in the magnitude and direction of the index n, which excludes a noticeable correlation in the $dP/dt(P)$ dependence.

With the same periods, when pulsars approach the "death line", they stop emitting, while their parameters $k \to \frac{2}{3}$ and $j \to \frac{1}{3}$, see Fig. 3. Thus, the pulsar ends its existence in the form of a pseudosphere at the highest density, i.e., at the largest evolutionary parameter ε, where

$$\varepsilon = f\, M_p^k\,, \tag{16}$$

(degenerate state; for more details see [2]).

The predicted nonsphericity of the pulsar is beginning to receive confirmation. Recent observations [13] have established that the location, shape, and size of hot regions on the surface of the pulsar PSR J0030+0451 cannot be explained by the canonical configuration of a globally centered dipole magnetic field.

4 Conclusion

Thus, geometrodynamic models are not only capable of explaining some currently poorly understood phenomena and features in planetary systems and pulsar spectra, but also of quantitatively calculating key pulsar parameters — their minimum luminosity ("death line") and braking indices. The results achieved indicate the need for further development of geometrodynamic models. In particular, it is necessary to replace the existing model underlying the theoretical study of pulsars with the one outlined above, supplementing it with specific observational data accumulated by specialists over the years of pulsar research, with the goal of refining and developing this model as a more physical model.

Submitted on August 14, 2026

References

1. Belyakov A. V. On some general regularities of formation of the planetary systems. *Progress in Physics*, 2014, v. 10, no. 1, 28–35.
2. Belyakov A. V. Evolution of stellar objects according to J. Wheeler's geometrodynamic concept. *Progress in Physics*, 2013, v. 9, no. 1, 25–40.
3. Dransfield G., Petit A. C., Triaud A., et al. ASTEP confirmation of a pair of long-period Jupiter-sized planets with extremely low densities transiting TOI-791. *Monthly Notices of the Royal Astronomical Society*, 2026, v. 549, issue 4, July 2026, stag864, 1–22.
4. Arriagada P., Anglada-Escud G. et al. Two planetary companions around the K7 dwarf GJ 221: a hot super-Earth and a candidate in the sub-Saturn desert range. arXiv: 1305.2203 (2013).
5. Malov I. F. Radio Pulsars. Nauka, Moscow, 2004 (*in Russian*).
6. Belyakov A. V. On the independent determination of the ultimate density of physical vacuum. *Progress in Physics*, 2011, v. 7, no. 2, 27–29.
7. Wu Q. D., Zhi Q. J., Zhang C. M., Wang D. H., Ye C. Q. Luminosity of radio pulsar and its new emission death line. arXiv: 2007.01015 (2020).
8. Farah J. R., Prust L. J., Howell D. A. Lense-Thirring precessing magnetar engine drives a superluminous supernova. *Nature*, 2026, v. 651, 321–325.
9. Malov I. F. and Marozava H. P. Parameter comparison of several types of pulsars. *Astronomy Reports — Russian Acad. Sci.*, 2020, v. 64, no. 9, 738–756.
10. Timirkeeva M. A. Study of the Characteristics of Radio Pulsars Emitting in the Gamma and X-Ray Ranges. Dissertation for the Degree of Candidate of Physical and Mathematical Sciences. Moscow, 2022 (*in Russian*).
11. Avramenko A. E., Losovsky B. Ya. Observational rotational stability of pulsars. Lebedev Physical Institute, Russian Academy of Sciences. *Astrometry-2015*, September 21–25, Pulkovo (*in Russian*).
12. Hewitt A. L., Pitkin M., Hook I. M. Recovering pulsar braking index from a population of millisecond pulsars. arXiv: 2412.10169 (2024).
13. Bilous A.V., Watts A.L., Harding A.K., et al. A NICER view of PSR J0030+0451: Evidence for a global-scale multipolar magnetic field. *The Astrophysical Journal Letters*, 2019, v. 887, no. 1, L23; arXiv: 1912.05704.